

# Transformation of topologically close-packed $\beta$ -W to body-centered cubic $\alpha$ -W: Comparison of experiments and computations

Katayun Barmak,<sup>1</sup> Jiaying Liu,<sup>1</sup> Liam Harlan,<sup>2</sup> Penghao Xiao,<sup>2</sup> Juliana Duncan,<sup>2</sup> and Graeme Henkelman<sup>2</sup>

<sup>1</sup>*Department of Applied Physics and Applied Mathematics, Columbia University, New York, New York 10027, USA*

<sup>2</sup>*Department of Chemistry and the Institute for Computational and Engineering Sciences, University of Texas at Austin, Austin, Texas 78712-0165, USA*

(Received 24 March 2017; accepted 7 July 2017; published online 27 July 2017)

The enthalpy and activation energy for the transformation of the metastable form of tungsten,  $\beta$ -W, which has the topologically close-packed A15 structure (space group  $Pm\bar{3}n$ ), to equilibrium  $\alpha$ -W, which is body-centered cubic (A2, space group  $Im\bar{3}m$ ), was measured using differential scanning calorimetry. The  $\beta$ -W films were 1  $\mu\text{m}$ -thick and were prepared by sputter deposition in argon with a small amount of nitrogen. The transformation enthalpy was measured as  $-8.3 \pm 0.4$  kJ/mol ( $-86 \pm 4$  meV/atom) and the transformation activation energy as  $2.2 \pm 0.1$  eV. The measured enthalpy was found to agree well with the difference in energies of  $\alpha$  and  $\beta$  tungsten computed using density functional theory, which gave a value of  $-82$  meV/atom for the transformation enthalpy. A calculated concerted transformation mechanism with a barrier of 0.4 eV/atom, in which all the atoms in an A15 unit cell transform into A2, was found to be inconsistent with the experimentally measured activation energy for any critical nucleus larger than two A2 unit cells. Larger calculations of eight A15 unit cells spontaneously relax to a mechanism in which part of the supercell first transforms from A15 to A2, creating a phase boundary, before the remaining A15 transforms into the A2 phase. Both calculations indicate that a nucleation and growth mechanism is favored over a concerted transformation. More consistent with the experimental activation energy was that of a calculated local transformation mechanism at the A15-A2 phase boundary, computed as 1.7 eV using molecular dynamics simulations. This calculated phase transformation mechanism involves collective rearrangements of W atoms in the disordered interface separating the A15 and A2 phases. *Published by AIP Publishing.* [<http://dx.doi.org/10.1063/1.4995261>]

## I. INTRODUCTION

Tungsten has seen significant interest in recent years for applications in both microelectronics and spintronics; the former using charge transport and the latter using spin transport based devices. In microelectronics, the continued downward scaling of transistor dimensions, in line with “Moore’s law,” has also required the scaling of the metallic interconnects.<sup>1</sup> This scaling of line dimensions down to and then below the room-temperature electron mean free path of 39 nm for copper—the current interconnect metal of choice—has resulted in a marked increase in resistivity.<sup>1–5</sup> This resistivity increase has in turn given rise to significant signal delay and power consumption, limiting the performance of integrated circuits. The International Technology Roadmap for Semiconductors (ITRS) has termed the resistivity-size effect in copper as a Grand Challenge problem, prompting consideration of alternate interconnect materials.<sup>1</sup>

One such candidate material for metallic interconnects is  $\alpha$ -W, which has the A2 or body-centered cubic crystal structure (bcc, space group  $Im\bar{3}m$ ).<sup>6,7</sup> Although the room-temperature bulk resistivity of  $\alpha$ -W at 5.3  $\mu\Omega$  cm is a factor of three larger than for Cu at 1.7  $\mu\Omega$  cm, its shorter electron mean free path of 19.1 nm, calculated using the Fermi

surface area obtained from density functional computations,<sup>7</sup> offers the possibility of a resistivity crossover below that of Cu at reduced line dimensions. Moreover, W offers the potential for improved reliability on account of its very much higher melting point of 3695 K compared with 1357 K for Cu, resulting in a higher activation barrier to diffusion and therefore lower susceptibility to failure by electromigration or stress voiding.<sup>7</sup>

However, challenges still need to be overcome—the deposition of W films, particularly at low temperatures relative to its melting point, which is required for interconnect fabrication, results in the formation of the  $\beta$ -W in addition to  $\alpha$ -W.<sup>6,8</sup>  $\beta$ -W has the topologically close-packed A15 structure (space group  $Pm\bar{3}n$ ) and has a resistivity that is 5–10 times higher than that of  $\alpha$ -W. Thus,  $\beta$ -W must be avoided in microelectronic applications, if W is to achieve the resistivity advantage over Cu in deeply scaled interconnects.

Yet, such avoidance is not universal—by contrast,  $\beta$ -W is the sought-after phase in spintronic devices based on the spin Hall effect (SHE). SHE refers to a family of spin-dependent transport phenomena caused by spin-orbit coupling in materials.<sup>9,10</sup> The SHE enables the conversion of charge current to pure spin current, even without the use of any ferromagnetic polarizer, making the SHE promising as the source of

spin-polarized current that can be manipulated by an electric field.<sup>11,12</sup>

The transfer efficiency of the charge-to-spin current is defined through the dimensionless figure of merit and the spin-Hall angle,  $\theta_{SH}$ . Among the elemental  $4d$  and  $5d$ -paramagnets for which  $\theta_{SH}$  has been measured, the highest room-temperature value reported is for  $\beta$ -W at  $\theta_{SH}^{\beta-W} = 0.3 \pm 0.02$ , prompting the recent interest in this metastable phase of tungsten.<sup>12</sup> In contrast, for  $\alpha$ -W, the spin-Hall angle is significantly lower ( $\theta_{SH}^{\alpha-W} < 0.07$ ). Studies have also shown that  $\theta_{SH}$  can vary over a wide range, depending on the deposition conditions and thus phase mixture of W.<sup>13,14</sup>

Given the large difference in properties between  $\alpha$ -W and  $\beta$ -W, the introduction of W into microelectronic and spintronic technology hinges upon being able to dictate the form of W (either  $\alpha$ -W or  $\beta$ -W) produced. This, in turn, requires a better understanding of formation and transformation processes for W. To this end, quantitative measure of the enthalpic stability of  $\alpha$ -W relative to  $\beta$ -W and insight into the transformation pathway(s) from  $\beta$  to  $\alpha$  are needed.

Recently, a promising method for preparation of  $\beta$ -W films that allows deposition of this phase with thicknesses as small as a few nanometers and as large as  $1 \mu\text{m}$  has been reported.<sup>15</sup> Micrometer-thick, free-standing films have been successfully used for thermodynamic and kinetic studies in a number of systems.<sup>16,17</sup> This approach is used in the current work to characterize the  $\beta$  to  $\alpha$  transformation of W. As will be shown, the experimentally measured transformation enthalpy compares well with the difference in the density functional theory computed energies of  $\beta$ -W relative to  $\alpha$ -W, validating the experimental methodology. It will however be shown that the experimentally measured activation barrier to the transformation is significantly lower than the activation barrier for lattice or grain boundary transport in W. To provide a physically plausible explanation for this lower barrier, simulations are used to determine the barrier for two transformation pathways: one of which is a concerted transformation mechanism and the other of which is a collective transport mechanism through a disordered interface. The better agreement between the activation barrier for the latter mechanism and the experimentally measured barrier points to transport through a disordered interface as the more physically plausible pathway for the growth of the beta phase. The experimentally measured barrier is also compared and contrasted with other experimental values reported in the literature. Based on this comparison, guidelines for dictating the phase of W that is formed are given.

## II. EXPERIMENTS AND COMPUTATIONS

### A. Experiments

The films for the study were prepared by sputter deposition at nominally room temperature onto 3-in. diameter oxidized Si(100) wafers with a 300-nm thick thermally grown oxide layer. The base pressure of the chamber prior to deposition was better than  $2 \times 10^{-8}$  Torr. To begin, a layer of Cu with a thickness of 300 nm was deposited by DC magnetron sputtering using 3 mTorr of Ar flowing at 20 SCCM. The Cu

layer acted as the sacrificial layer for the lift-off of the tungsten films. A 100-nm thick layer of silicon dioxide was deposited next by RF magnetron sputtering using the same Ar pressure and flow rate. Next, the  $1 \mu\text{m}$ -thick  $\beta$ -W layer was deposited on the  $\text{SiO}_2$  underlayer using 3 mTorr Ar gas as the sputtering gas along with nitrogen introduced into the chamber through the load-lock chamber. Prior work had shown that the introduction of nitrogen during sputter deposition of tungsten promotes the formation of  $\beta$ -W phase.<sup>15</sup> The  $\text{N}_2$  pressure was calibrated in the absence of Ar by filling the load-lock chamber to a given pressure and determining the nitrogen pressure in the deposition chamber at the steady-state leak rate through the gate valve separating the deposition chamber from the load-lock chamber. The  $\text{N}_2$  pressure in the deposition chamber was  $1.2 \times 10^{-5}$  Torr for the current study.<sup>15</sup>

Following the deposition of the trilayer stack of  $\text{Cu}/\text{SiO}_2/\beta$ -W and prior to lift-off to generate free-standing films for DSC measurements, the films were examined by  $\theta$ - $2\theta$  X-ray diffraction (XRD) scans. The scans were done out-of-plane, i.e., with the scattering vector normal to the film plane, using a Rigaku Ultima III diffractometer at the Center for Functional Nanomaterials at Brookhaven National Laboratory.

Free-standing  $\text{SiO}_2/\beta$ -W bilayer flakes were obtained by dissolving the Cu layer in nitric acid. The flakes were rinsed in distilled water, acetone, and isopropyl alcohol. The  $\text{SiO}_2$  layer was then removed by dipping the flakes in 49% hydrofluoric acid. The resulting  $1 \mu\text{m}$ -thick free-standing  $\beta$ -W flakes were again cleaned in distilled water, acetone, and isopropyl alcohol and allowed to fully dry prior to calorimetric studies.

The  $\beta$ - to  $\alpha$ -W phase transition was studied with differential scanning calorimetry (DSC) conducted in a Perkin-Elmer DSC-7. The instrument was calibrated for temperature and thermal lag using standard reference materials. Approximately 5 mg of the  $\beta$ -W flakes was encapsulated in a Pt foil that acted as a sample pan. An empty Pt foil was used in the reference pan to match as closely as possible the heat capacity of the sample and reference furnaces. The DSC experiments were conducted with heating rates of 20, 40, 60 and 80  $^\circ\text{C}/\text{min}$  under flowing ultrahigh purity Ar in the temperature range 50–700  $^\circ\text{C}$ . Two consecutive DSC measurements of the same specimen were performed under the same conditions, in order to obtain a baseline for the extraction of the heat flow associated with the  $\beta$ -W to  $\alpha$ -W phase transformation.

### B. Computations

The density functional theory (DFT) calculations were performed with the Vienna *Ab initio* Simulation Package (VASP). The Perdew–Burke–Ernzerhof (PBE) functional was used to describe the exchange correlation energy. Tests with the PW91 and PBEsol functionals show that our results are insensitive to the specific functional used, as described later. Valence electron wave functions were expanded in a plane wave basis set with an energy cutoff of 300 eV; their interaction with core electrons was modeled within the projector augmented wave framework. An eight-atom A15 unit cell, with a lattice parameter of 5.05  $\text{Å}$ , was used to represent the initial  $\beta$ -W state of the phase transition. The Brillouin zone was sampled with a

$5 \times 5 \times 5$  K-point mesh using the Monkhorst-Pack scheme. Energies were converged to within  $10^{-5}$  eV, and geometries were considered converged when the maximum force on every atom was below  $0.01$  eV/Å. The concerted solid-solid phase transition mechanism between  $\beta$ -W and  $\alpha$ -W was calculated with DFT using the solid-state nudged elastic band method.<sup>18</sup> This transition was also calculated using an embedded atom method (EAM) interatomic potential<sup>19</sup> for both the A15 unit cell and a  $2 \times 2 \times 2$  supercell. The supercell calculation indicated the spontaneous emergence of an  $\alpha$ -W nucleation event and the propagation of the  $\alpha$ -W phase through the  $\alpha/\beta$  phase boundary.

To investigate the growth of the  $\alpha$  phase, molecular dynamics calculations were used to examine local transformation mechanisms at the  $\alpha/\beta$  phase boundary. For these calculations, the LAMMPS and EON codes<sup>20,21</sup> were used with the EAM interatomic potential.<sup>19</sup> The system studied contains a phase boundary between the bcc  $\alpha$ -W and the A15  $\beta$ -W phases. The supercell is shown in Fig. 1(a) where 8  $\alpha$ -W unit cells are matched with 5  $\beta$ -W unit cells in the  $x$  and  $y$  directions. The lateral size of the cell, fixed at  $25.43$  Å, as well as the  $39.42$  Å cell length in the  $z$  direction, was selected to minimize the strain placed on the  $\alpha$ -W and the  $\beta$ -W phases [Fig. 1(b)]. The cell was modeled with periodic boundary conditions so the atoms furthest from the interface were frozen [green atoms shown in Fig. 1(a)]. A larger supercell (not shown), doubled in the  $x$  and  $y$  directions, was used to test for system size effects.

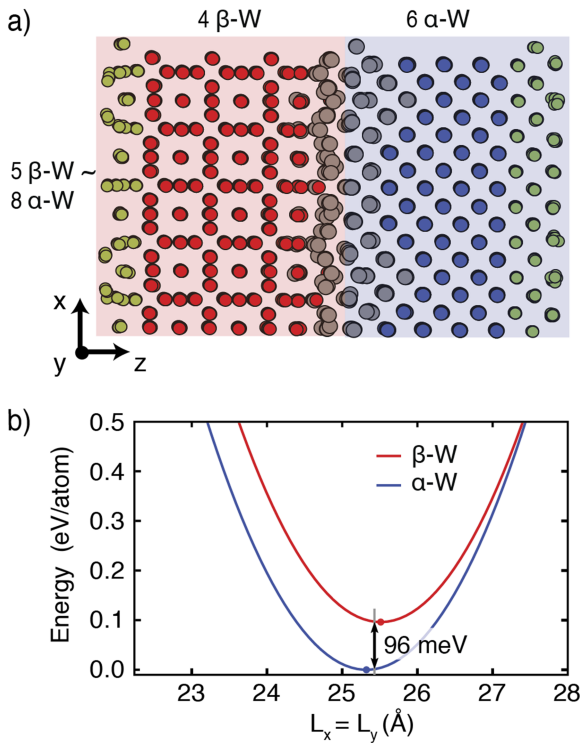


FIG. 1. (a) An illustration of the system setup used. An  $8 \times 8 \times 6$  set of  $\alpha$ -W unit cells was paired with a  $5 \times 5 \times 4$  set of  $\beta$ -W unit cells. The green atoms represent atoms fixed in the simulation, the red atoms represent  $\beta$ -W, the blue atoms represent  $\alpha$ -W, and the grey atoms are at the interface. (b) Energy versus the  $x$ - $y$  lattice constants with a fixed  $z$  lattice constant. The chosen lattice constant is the average between the optimal values for  $\alpha$ -W and  $\beta$ -W. The driving force is 96 meV/atom favoring  $\alpha$ -W. See text for more details.

High temperature molecular dynamics simulations were performed within the NVT ensemble using the Anderson thermostat with a collision period of 600 fs to ensure constant temperature. An integration time step of 5 fs was used. The location of the  $\alpha$ - $\beta$  interface was tracked over time using a common neighbor analysis (CNA)<sup>22</sup> whereby each atom in the system was identified within the  $\alpha$ -W and  $\beta$ -W phases, or part of the disordered interface. The interface position was defined by the  $z$ -coordinate of the disordered atom closest to the  $\alpha$ -W phase. Mean first passage times,  $\bar{\tau}_{layer}$ , were used to calculate the rate,  $k = 1/\bar{\tau}_{layer}$ , for layers of  $\beta$ -W to transform into the  $\alpha$ -W phase.

### III. RESULTS AND DISCUSSION

The XRD pattern of the thermally oxidized Si(100) substrate and deposited stack structure, Si(100)/SiO<sub>2</sub>/Cu/SiO<sub>2</sub>/W, is shown in Fig. 2. The presence of  $\beta$ -W phase is indicated by its (200), (210), and (211) diffraction peaks. The (200) peak of  $\alpha$ -W at about  $2\theta = 58^\circ$  is not observed in the XRD pattern, from which it is concluded that no  $\alpha$ -W is formed and the tungsten layer is fully  $\beta$ -W in agreement with our prior work for the given pressure of N<sub>2</sub> in the deposition chamber.<sup>15</sup>

The DSC curves for the  $\beta$ -W film from two consecutive measurements of the same specimen at the heating rate of  $40$  °C/min are shown in Fig. 3. The exothermic peak at about  $600$  °C seen in the first scan is attributed to the  $\beta$ -W to  $\alpha$ -W phase transition. Figure 4 presents the baseline-subtracted traces at four heating rates. The peak temperatures for these DSC traces are listed in Table I. To obtain the molar value of the transformation enthalpy, the areas under the peaks in Fig. 4 are determined by integration with respect to time,

$$\Delta H^{\beta \rightarrow \alpha} = \int \frac{1}{\beta} \frac{d\Delta H}{dT} dt, \quad (1)$$

where  $\beta = \frac{dT}{dt}$  is the heating rate and  $\frac{d\Delta H}{dT}$  is the measured heat flow signal. Using these integrated areas and the molecular mass of tungsten, the  $\beta$  to  $\alpha$  transformation enthalpy is

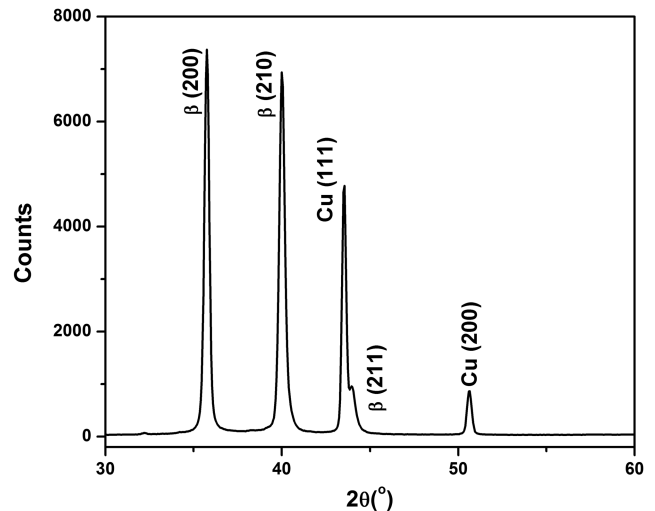


FIG. 2. The XRD pattern of the as-deposited Cu/SiO<sub>2</sub>/ $\beta$ -W trilayer on a thermally-oxidized Si(100) substrate.

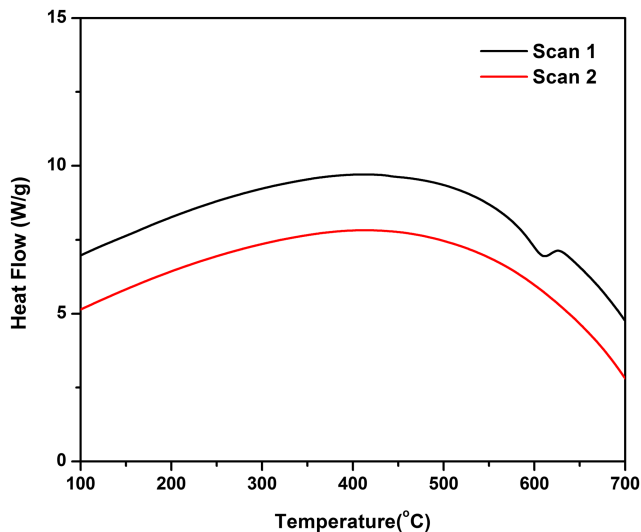


FIG. 3. The DSC traces of  $\beta$ -W at a heating rate of 40 °C/min. Scan 2 represents the baseline. The curves are displaced for clarity.

calculated per mole of atoms as  $-8.3 \pm 0.4$  kJ/mol ( $86 \pm 4$  meV/atom).

This experimentally measured transformation enthalpy can be compared with computed values. Figure 5 shows the minimum energy pathway for the concerted phase transition between  $\beta$ -W and  $\alpha$ -W calculated using density functional theory (DFT). The endpoint energies give the calculated transformation enthalpy of  $-7.9$  kJ/mol ( $-82$  meV/atom). DFT computed energies of  $\beta$ -W and  $\alpha$ -W have also been reported previously and can be found in the Materials Project Database, which give a value of  $-8.7$  kJ/mol ( $-90$  meV/atom) for the transformation enthalpy.<sup>23</sup> We also calculated the transformation enthalpy using the PW91 functional ( $-81$  meV/atom) and the PBEsol functional ( $-87$  meV/atom), to test for sensitivity of our DFT calculations with respect to the functional. Within experimental error, the experimentally measured enthalpy compares remarkably well with these DFT computed

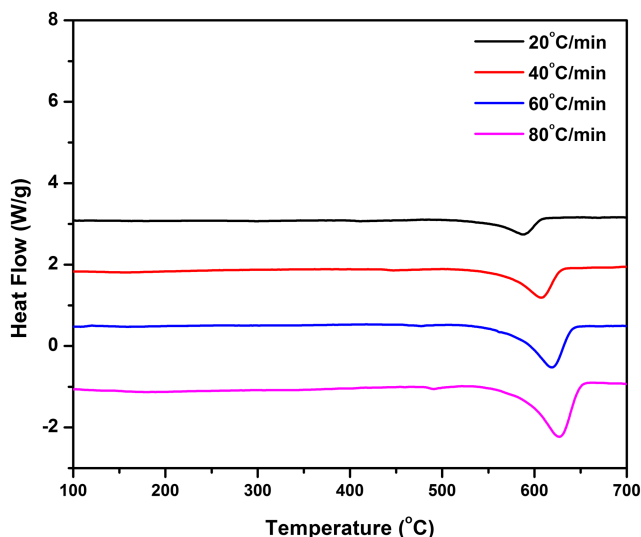


FIG. 4. Baseline-subtracted DSC curves of  $\beta$ -W measured at different heating rates. The curves are displaced for clarity.

TABLE I. DSC peak temperatures at different heating rates. The DSC traces are given in Fig. 4.

$\beta$ (°C/min)	$T_{peak}$ (°C)
20	587
40	607
60	619
80	627

values, thereby lending validity to the thin film synthesis and calorimetric methodologies used here.<sup>15,16</sup>

With regard to transformation kinetics, the exothermic peaks for the  $\beta$ -W to  $\alpha$ -W phase transformation in Fig. 2 are seen to shift to higher temperatures with increasing heating rate, thereby indicating that the transformation is thermally activated. The activation energy,  $Q$ , for the transition can be extracted from the peak shifts using the Kissinger method<sup>24</sup> according to Eq. (2) as

$$\ln \frac{k_B A}{Q} - \frac{Q}{k_B T_{peak}} = \ln \frac{\beta}{T_{peak}^2}, \quad (2)$$

where  $T_{peak}$  is the peak temperature of the baseline-subtracted trace for the given heating rate  $\beta$ . A plot of  $\ln \frac{\beta}{T_{peak}^2}$  vs.  $\frac{1}{k_B T_{peak}}$  should give a straight line whose slope is the (negative of the) effective activation energy  $Q$  of the phase transformation. This plot is shown in Fig. 6, using the peak temperatures listed in Table I. The activation energy of  $\beta$ - to  $\alpha$ -W phase transformation is determined from the slope as  $2.2 \pm 0.1$  eV. This activation energy is an effective energy for all the processes associated with the transformation, including the nucleation of the  $\alpha$  phase in addition to its growth.

To gain insight into the transformation pathway(s), it is useful to compare the measured activation energy with activation energies for lattice and grain boundary diffusion in W. Lattice diffusion occurs by vacancy migration through the volume of the crystal, while grain boundary diffusion occurs by

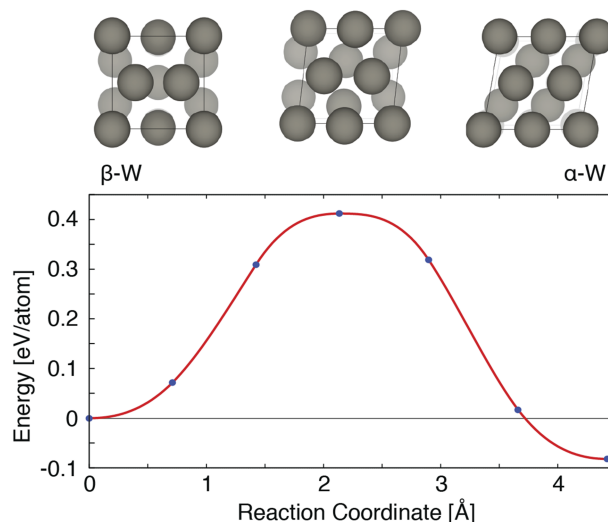


FIG. 5. Minimum energy path for the concerted solid-solid phase transition between a unit cell of  $\beta$ -W and  $\alpha$ -W. The transition has a barrier of 0.4 eV/atom.

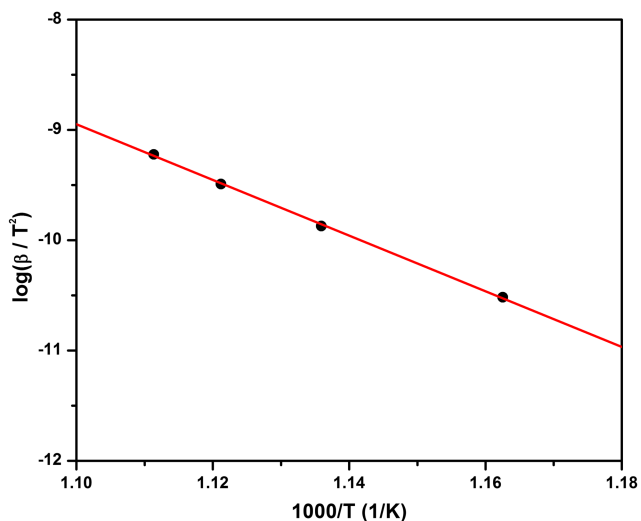


FIG. 6. The plot of  $\ln \frac{\beta}{T^2}$  vs.  $\frac{1}{k_B T_{peak}}$  using the peak temperatures and heating rates of DSC measurements listed in Table I. The activation energy of A15  $\beta$ -W to A2  $\alpha$ -W phase transformation is determined from the slope of the plot as  $2.2 \pm 0.1$  eV.

atom migration along the more open structure of the boundary shared by two adjacent crystallites. For W, the reported values are 7 and 4 eV, respectively.<sup>25,26</sup> These two values are significantly larger than the experimentally measured activation energy for the overall transformation of 2.2 eV. Therefore, the  $\beta$  to  $\alpha$  transformation in the current study must be occurring via a mechanism with a lower activation barrier for the growth of  $\alpha$  from the metastable parent  $\beta$ . The two mechanisms investigated in the current work are discussed below.

The concerted phase transformation mechanism, depicted in Fig. 5, which involves both atomic motion and a change in the cell vectors, has an activation energy of 0.4 eV/atom. This DFT calculation was done starting from the  $\beta$ -W A15 unit cell depicted. In the concerted mechanism, all the atoms in the unit cell move collectively with the cell parameters to form the  $\alpha$ -W A2 structure. An important aspect of a concerted mechanism is that the actual energy barrier scales directly with the number of atoms involved in the phase transformation. By comparing the per-atom activation energy of 0.4 eV/atom in the concerted mechanism to the experimentally observed activation energy of 2.2 eV, we can conclude that the concerted mechanism would only be consistent with the experiment for a critical nucleus of only five atoms, or a mere two unit cells of bcc  $\alpha$ -W, each with two atoms per unit cell. A critical nucleus of only two unit cells is far too small to be physically plausible.

In order to test this reasoning, we have also preformed a calculation of the concerted mechanism with a significantly larger supercell consisting of eight A15 unit cells, as shown in Fig. 7. For this supercell calculation, we used the EAM empirical potential. The concerted mechanism for a unit cell, using the EAM potential, is comparable to the DFT calculation with a barrier of 0.31 eV/atom and a reaction enthalpy of  $-0.1$  eV/atom. Interestingly, when the cell is increased to a  $2 \times 2 \times 2$  supercell, the barrier of the concerted mechanism, involving all atoms, scales with the number of atoms so

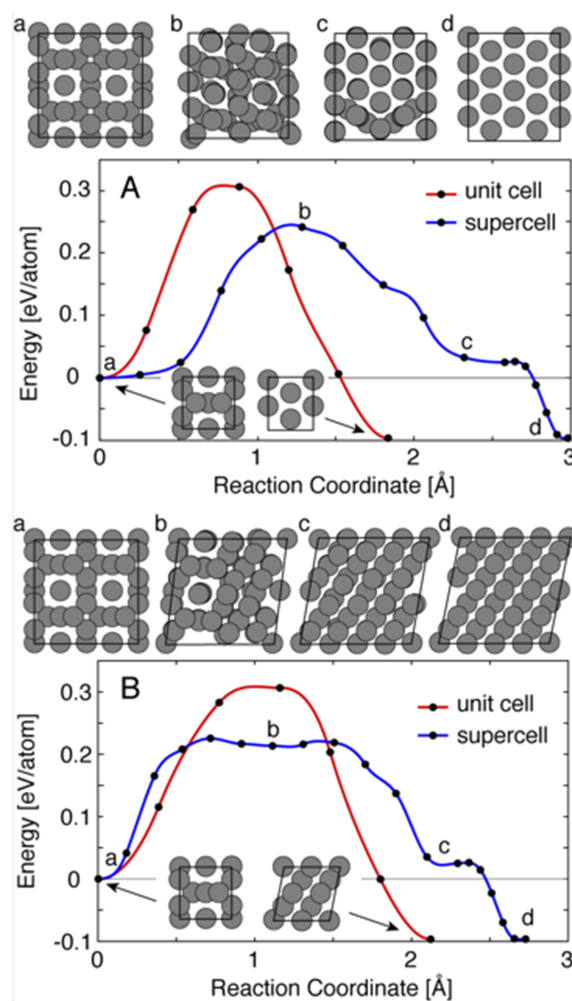


FIG. 7. Minimum energy pathways, calculated using an embedded atom method force field, for the transition between  $\beta$ -W and  $\alpha$ -W in a supercell containing eight A15 unit cells (blue) as compared with a single A15 unit cell (red). Both transitions show a relaxation of the concerted mechanism in the supercell into a lower energy transformation of an  $\alpha$ -W phase and then motion of the  $\alpha/\beta$  phase boundary to form  $\alpha$ -W.

that lower energy mechanisms, involving just a subset of the atoms, can become favorable (see Ref. 27). Figure 7 shows two such mechanisms corresponding to different final states, differentiated by the corresponding identity of the atoms in the  $\alpha$  and  $\beta$  structures. For both pathways, the minimum energy pathway spontaneously relaxes into a two-step process involving first the formation of an  $\alpha$ -W phase and then the propagation of the  $\alpha/\beta$  phase boundary to form a complete  $\alpha$ -W structure. These calculations confirm that the concerted mechanism is not the active mechanism at the experimentally relevant temperatures of  $\sim 1000$  K, and that it is rather the propagation of the  $\alpha$ -W phase through the  $\alpha/\beta$  phase boundary.

The second possible mechanism for the formation of the  $\alpha$ -W phase is for the  $\beta$  to  $\alpha$  transformation to take place via local atomic rearrangements at their phase boundary. This growth of the  $\alpha$ -W phase was modeled by MD of an interface between the  $\alpha$ -W and  $\beta$ -W phases. Figure 8 shows the change in potential energy and interface location over time for a typical MD simulation of this local phase transition. As the simulation progresses, potential energy is gained as the bcc

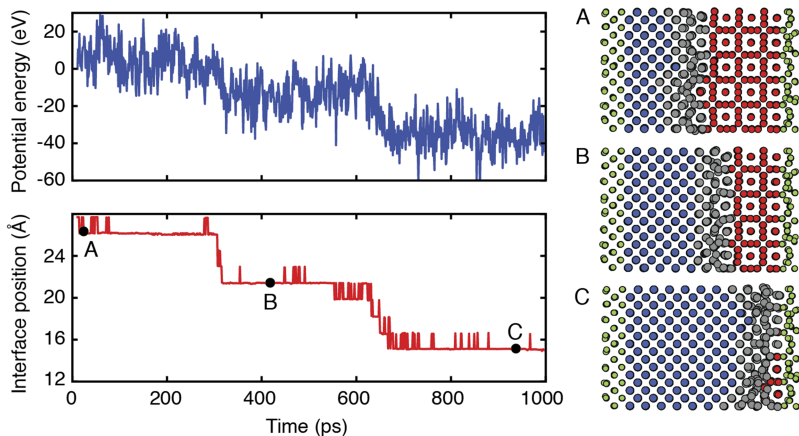


FIG. 8. The potential energy and interface location over time during an MD trajectory at 2250 K and snapshots of the MD trajectories at the three plateaus seen in all MD trajectories.

$\alpha$ -W phase forms. Plateaus in the potential energy correspond to relatively stable interface structures between the phases. The rapid drop in energy between plateaus corresponds to the advance of the disordered layer into the  $\beta$ -W phase and a subsequent ordering of atoms in the phase boundary into a new layer of  $\alpha$ -W. The transformation of a layer of  $\beta$ -W to  $\alpha$ -W results in an energy drop of 0.096 eV/atom (19.2 eV per layer). The per-layer phase transformation rate was calculated from an average, over 30 trajectories, of the time between the loss of A15  $\beta$ -W layers. To avoid any bias as a result of our initial structure, we allowed the system to equilibrate from our initial conditions while the first A15 layer transformed and then averaged just the transformation time for the second A15 layer. From MD rates corresponding to temperatures ranging from 3000 K to 1750 K, an activation energy of 1.7 eV was found for the transformation of a single of  $\beta$ -W layer to  $\alpha$ -W (see Fig. 9). To test for system size effects, layer transformation rates were also calculated for a larger system with 16  $\alpha$ -W and 10  $\beta$ -W unit cells in the  $x$  and  $y$  planes. The activation energy for a layer transition in this larger cell, 1.4 eV, was marginally lower, giving some measure of the uncertainty in our MD calculations.

The local mechanism, while having an activation energy somewhat lower than measured experimentally, provides a

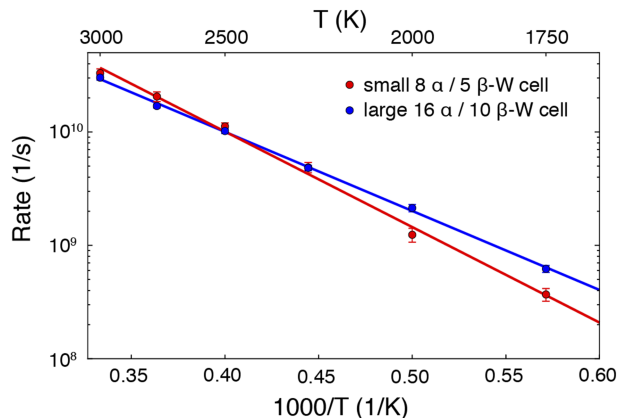


FIG. 9. Arrhenius plot of the rate of the removal of an A15 layer taken from MD simulations performed between 3000 K and 1750 K. An activation energy of 1.7 eV was found for the initial, “small,” system (with 8  $\times$  8  $\alpha$ -W and 5  $\times$  5  $\beta$ -W atoms in the  $x$ - $y$  plane shown in Fig. 1), and 1.4 eV for a “large” system with 16  $\times$  16  $\alpha$ -W and 10  $\times$  10  $\beta$ -W atoms in the  $x$ - $y$  plane.

more reasonable picture of the phase transformation process. There are a number of possible reasons that may explain the difference in these values. One is that the experimental value includes the activation barrier to nucleation in addition to the barrier for growth. However, given the spontaneous nucleation of the alpha phase in larger simulation cells (Fig. 7), this seems unlikely. A second reason may be that the activation barrier for the transformation may be temperature dependent. Experimentally, the transformation is seen to occur at measurable rates in the temperature range of 500-650 °C (<1000 K), whereas the MD simulations are conducted in the temperature range of 1750-3000 K. However, given that both the experimental and MD activation barriers are lower than the reported barriers for lattice and grain boundary diffusion, it is reasonable to conclude that the displacements required to mediate the transformation are less locally distortive than normal diffusional processes.

Finally, it is useful to compare the experimentally measured activation barrier in the current work with other experimental reports in the literature and to use this comparison to provide guidelines for dictating the phase of W that is formed during film deposition.<sup>6,8,28–34</sup> For W films deposited by plasma enhanced chemical vapor deposition (PECVD), Tang and Hess<sup>32</sup> reported a value of 0.75 eV for the activation barrier for the  $\beta$  to  $\alpha$  transformation. For RF sputtered W films, Petroff *et al.*<sup>30</sup> also reported a value of 0.75 eV, whereas for DC sputtered films, Rosnagel *et al.*<sup>8</sup> reported a value of 1.1  $\pm$  0.2 eV. These values are all significantly lower than the activation energy of 2.2  $\pm$  0.1 eV obtained in the current work, a point that will be discussed further below.

In many of the prior studies of W deposition, the formation of  $\beta$ -W phase was achieved by deliberately introducing oxygen into the chamber (see, for example, Ref. 35) when  $\beta$  was the desired phase, or was the unwanted consequence of the presence of residual oxygen impurities in the chamber when  $\alpha$  was the desired phase (see, for example, Ref. 6). In either case, the formation of the  $\beta$  phase was limited to only a few nanometers. For example, in the work of Rosnagel *et al.*,<sup>8</sup> films with thicknesses below 5 nm were mostly  $\beta$ -W. Film thicknesses in the 5-45 nm range were a mixture of A15  $\beta$ -W and A2  $\alpha$ -W. Films above 45 nm were only  $\alpha$ -W. These films should be contrasted with the films in the current study, which are fully  $\beta$ -W at a thickness of 1  $\mu$ m.

Based on the results of the current work, we conclude that the limited thickness of the beta phase in prior studies was a consequence of the fact that oxygen, although it can promote the formation of the  $\beta$  phase, does not fully suppress the nucleation of the  $\alpha$  phase. Thus, at some point during film deposition, the  $\beta$  phase begins to transform to  $\alpha$ . Remarkably, this transformation can occur at room temperature. For example, the  $\beta$ -W phase in the films of Rosnagel *et al.* transformed at room temperature to  $\alpha$ -W over a period of hours to days. In contrast, the films in the current study require heating to temperatures beyond 500 °C for the transformation to occur at measurable rates. We believe this to be a result of the fact that by introducing nitrogen instead of oxygen into the chamber, the nucleation of  $\alpha$  is suppressed, so long as the amount of nitrogen introduced is enough and that there is adequate surface coverage of the adsorbed nitrogen on the deposition surface. This last statement is based on our prior observation that the variation of the fraction of  $\beta$  with nitrogen pressure follows the Langmuir-Freundlich isotherm.<sup>15</sup>

If nuclei of  $\alpha$ -W are prevented from forming during the deposition, the  $\beta$  tungsten film is stable up to several hundred degrees, as demonstrated in the current work. This can also explain the higher value by a factor of two or larger of the activation energy obtained in the current work compared to prior reports listed above. In the current work, thermally activated nucleation of  $\alpha$  is required for the transformation to proceed, whereas in prior studies, nuclei of the  $\alpha$  phase were already present in the deposited films, and the measured activation energies were only a measure of the barrier to the growth of the  $\alpha$  phase.

Based on the above discussion, in order to dictate the formation of  $\alpha$  vs.  $\beta$ , the following must be done. If  $\alpha$  is the desired phase, then all residual oxygen must be eliminated from the deposition chamber to prevent nucleation of  $\beta$ . By contrast, if  $\beta$  is the desired phase, then adequate quantities of nitrogen must be introduced into the chamber and must adsorb on the depositing surface with enough coverage to suppress nucleation of the  $\alpha$  phase.

#### IV. CONCLUSIONS

Calorimetric measurements of free-standing, 1  $\mu$ m-thick films of  $\beta$ -W gave enthalpy and activation energy values for the  $\beta$  to  $\alpha$  (A15 to A2) transition of  $-8.3 \pm 0.4$  kJ/mol ( $86 \pm 4$  meV/atom) and  $2.2 \pm 0.1$  eV, respectively. The transformation enthalpy showed good agreement with the DFT computed transformation enthalpy value of  $-82$  meV/atom. The experimentally measured activation energy was found to be inconsistent with a calculated concerted transformation mechanism with a barrier of 0.4 eV/atom for any critical nucleus larger than two A2 unit cells. Calculations of this transition with larger supercells show a spontaneous relaxation from a concerted mechanism to a lower energy nucleation and growth process. More consistent with the experimental activation energy was that of a phase transformation mechanism that involved collective rearrangements of W atoms in the disordered interface separating the A15 and A2 phases, with a MD computed activation energy of 1.7 eV. The

activation energies determined experimentally and by MD simulations are significantly lower than the reported activation energies for lattice and grain boundary diffusion in  $\alpha$ -W.

#### ACKNOWLEDGMENTS

Partial funding support under NSF No. DMR-1411160 is gratefully acknowledged. Parts of the research were carried out at the Center for Functional Nanomaterials, Brookhaven National Laboratory, which is supported by the U.S. Department of Energy, Office of Basic Energy Sciences, under Contract No. DE-SC0012704. The computational work was supported by the Welch Foundation under Grant No. F-1841 and the Texas Advanced Computation Center. We would like to acknowledge Christienne Te and the other students in the Freshman Research Initiative who conducted molecular dynamics simulations.

<sup>1</sup> See <http://www.itrs2.net/> for the roadmap for interconnects in semiconductor technology.

<sup>2</sup> J. J. Thomson, Proc. Cambridge Philos. Soc. **11**, 120 (1901).

<sup>3</sup> F. Chen and D. Gardner, *IEEE Electron Device Lett.* **19**, 508 (1998).

<sup>4</sup> D. Josell, S. H. Brongersma, and Z. Tǒkci, *Annu. Rev. Mater. Res.* **39**, 231 (2009).

<sup>5</sup> T. Sun, B. Yao, A. P. Warren, K. Barmak, M. F. Toney, R. E. Peale, and K. R. Coffey, *Phys. Rev. B* **81**, 155454 (2010).

<sup>6</sup> D. Choi, K. Barmak, A. Darbal, X. Liu, A. Warren, and K. R. Coffey, *J. Vac. Sci. Technol., A* **29**, 051512 (2011).

<sup>7</sup> D. Choi, C.-S. Kim, S. Chung, A. P. Warren, N. T. Nuhfer, M. F. Toney, K. R. Coffey, and K. Barmak, *Phys. Rev. B* **86**, 045432 (2012).

<sup>8</sup> S. M. Rosnagel, I. C. Noyan, and C. Cabral, *J. Vac. Sci. Technol., B: Microelectron. Nanometer Struct.* **20**, 2047 (2002).

<sup>9</sup> J. Hirsch, *Phys. Rev. Lett.* **83**, 1834 (1999).

<sup>10</sup> S. Valenzuela and M. Tinkham, *Nature* **442**, 176 (2006).

<sup>11</sup> T. Jungwirth, J. Wunderlich, and K. Olejnik, *Nat. Mater.* **11**, 382 (2012).

<sup>12</sup> C.-F. Pai, L. Liu, Y. Li, H. W. Tseng, D. C. Ralph, and R. A. Buhrman, *Appl. Phys. Lett.* **101**, 122404 (2012).

<sup>13</sup> J. Liu, T. Ohkubo, S. Mitani, K. Hono, and M. Hayashi, *Appl. Phys. Lett.* **107**, 232408 (2015).

<sup>14</sup> C. Zhang, S. Fukami, K. Watanabe, A. Ohkawara, S. DuttaGupta, H. Sato, F. Matsukura, and H. Ohno, *Appl. Phys. Lett.* **109**, 192405 (2016).

<sup>15</sup> J. Liu and K. Barmak, *Acta Mater.* **104**, 223 (2016).

<sup>16</sup> C. Michaelsen, K. Barmak, and T. P. Weihs, *J. Phys. D: Appl. Phys.* **30**, 3167 (1997).

<sup>17</sup> B. Wang, D. C. Berry, Y. Chiari, and K. Barmak, *J. Appl. Phys.* **110**, 013903 (2011).

<sup>18</sup> D. Sheppard, P. Xiao, W. Chemelewski, D. D. Johnson, and G. Henkelman, *J. Chem. Phys.* **136**, 074103 (2012).

<sup>19</sup> X. W. Zhou, R. A. Johnson, and H. N. G. Wadley, *Phys. Rev. B* **69**, 144113 (2004).

<sup>20</sup> S. T. Chill, M. Welborn, R. Terrell, L. Zhang, J.-C. Berthet, A. Pedersen, H. Jónsson, and G. Henkelman, *Modell. Simul. Mater. Sci. Eng.* **22**, 055002 (2014).

<sup>21</sup> S. Plimpton, *J. Comput. Phys.* **117**, 1 (1995), software available at <http://lammps.sandia.gov/>.

<sup>22</sup> A. S. Clarke and H. Jónsson, *Phys. Rev. E* **47**, 3975 (1993).

<sup>23</sup> A. Jain, S. P. Ong, G. Hautier, W. Chen, W. D. Richards, S. Dacek, S. Cholia, D. Gunter, D. Skinner, G. Ceder, and K. A. Persson, *APL Mater.* **1**, 011002 (2013).

<sup>24</sup> H. E. Kissinger, *Anal. Chem.* **29**, 1702 (1957).

<sup>25</sup> J. N. Mundy, S. J. Rothman, N. Q. Lam, H. A. Hoff, and L. J. Nowicki, *Phys. Rev. B* **18**, 6566 (1978).

<sup>26</sup> J. S. Lee, C. Minkwitz, and C. Herzig, *Phys. Status Solidi B* **202**, 931 (1997).

<sup>27</sup> P. Xiao, D. Sheppard, J. Rogal, and G. Henkelman, *J. Chem. Phys.* **140**, 174104 (2014).

<sup>28</sup> A. Miller and G. D. Barnett, *J. Electrochem. Soc.* **109**, 973 (1962).

<sup>29</sup> S. Basavaiah and S. R. Pollack, *J. Appl. Phys.* **39**, 5548 (1968).

- <sup>30</sup>P. Petroff, T. T. Sheng, A. K. Sinha, G. A. Rozgonyi, and F. B. Alexander, *J. Appl. Phys.* **44**, 2545 (1973).
- <sup>31</sup>W. R. Morcom, W. L. Worrell, H. G. Sell, and H. I. Kaplan, *Metall. Trans.* **5**, 155 (1974).
- <sup>32</sup>C. Tang and D. W. Hess, *Appl. Phys. Lett.* **45**, 633 (1984).
- <sup>33</sup>H. H. Busta and C. H. Tang, *J. Electrochem. Soc.* **133**, 1195 (1986).
- <sup>34</sup>C. Paine, J. C. Bravman, and C. Y. Yang, *Appl. Phys. Lett.* **50**, 498 (1987).
- <sup>35</sup>A. J. Narasimham, M. Medikonda, A. Matsubayashi, P. Khare, H. Chong, R. J. Matyi, A. Diebold, and V. P. LaBella, *AIP Adv.* **4**, 117139 (2014).